Modeling of composite and sandwich beams with a generic cross-section using a variable separation method

P. Vidal, G. Giunta, Laurent Gallimard, Olivier Polit

Modeling of composite and sandwich beams with a generic cross-section using a variable separation method

P. Vidal[a,*], G. Giunta[b], L. Gallimard[a], O. Polit[a]

[a] LEME, UPL, Univ Paris Nanterre, 92410, Ville d'Avray, France
[b] Luxembourg Institute of Science and Technology, 5, Avenue des Hauts-Fourneaux, L-4362, Esch-sur-Alzette, Luxembourg

ARTICLE INFO

Keywords:
Generic cross-section
Composite beam
Variable separation method
Finite element solution

ABSTRACT

In this work, the modeling of laminated composite and sandwich beams with a generic cross-section is performed through a variable separation approach. For this purpose, the displacement is approximated as a sum of separated functions of the cross-section coordinates y, z and the axial coordinate x. This choice yields to a non-linear problem that can be solved by an iterative process. This latter consists of solving a 2D and 1D Finite Element problem successively at each iteration.

Numerical examples involving several representative sandwich and laminated beams are addressed to show the accuracy of the present method. It is shown that it can provide 3D results and capture local effects for various types of cross-section.

1. Introduction

Beam-like elements are very important structures since they find several applications in different engineering fields for aeronautic, space, civil and energy applications. Current needs in terms of performances per unit mass call for materials with improved properties such as fibre reinforced laminated and sandwich materials. As a counterpart, the resulting structural mechanical response is much more complex than in the case of beams made of classical materials. Accurate yet computational attractive modeling strategies are, therefore, required making composite structures modeling an actual research field. In this way, note the substantial works related to the so-called Carrera's Unified Formulation (CUF) applied to the beam structures [1–3]. It allows to implement easily hierarchical models from classical to higher-order beam theories. The number of unknown variables is a free parameter of the problem. Model reduction techniques are an attractive approach to contain the computational costs with an acceptable, or even negligible, loss of accuracy. In this sense, a variable separation technique based on a Proper Generalized Decomposition (PGD) to divide the approximation space into coupled lower dimensional ones was proposed by Ammar et al. [4,5] for fluid dynamic applications. The method is a natural extension of the radial approximation in the framework of the LArge Time INcrement strategy (also known as LATIN method, see Ladevèze [6]). In this latter, space coordinates are separated from time. Néron and Ladevèze [7] presented a review of the coupled use of LATIN and PGD methods for multi-scale and multi-physics problems. They also briefly addressed the main differences with methods based upon a Proper Orthogonal Decomposition (POD). PGD does not require any a priori knowledge of the solution whereas a partial solution, or "snapshot" is needed in the case of POD. Also, a refined solution is less expensive in PGD that for POD. A more comprehensive comparison between POD and PGD can be found in Chinesta and Ladevèze [8]. The PGD approach has been, then, used in several fields in Physics and Engineering such as, for instance, quantum mechanics, computational rheology, stochastic analyses, composite manufacturing processes and real time simulations for computational surgery, see Nouy [9], Chinesta et al. [10,11] and Quesada et al. [12,13]. Different flavours of PGD methods were discussed by Nouy [14] for solving time dependent partial differential equations. As an alternative to "brute force" simulation approaches, Chinesta et al. [15] introduced the concept of *computational vademecum* by considering that extra-coordinates, such as problem specific parameters, can be added to the time and space ones to obtain a multi-dimensional problem that can be solved in one run. The obtained solution, then, can be used for optimisation, uncertainty quantification real-time simulation and combination of off-line solution with real-time querying on small portable devices. In this sense, a multi-parametric solution for the modeling of materials, structures and processes was presented in Chinesta and Cueto [16]. Vitse et al. [17] obtained virtual charts for parametrized time depended non-linear problems by means of a LATIN-PGD coupled

* Corresponding author.
E-mail address: philippe.vidal@parisnanterre.fr (P. Vidal).

approach. In assessing the separability of a solution as far as its manifold structure is concerned, Badias et al. [18] proposed three versions of a local proper generalized decomposition method for estimating the size of the solution manifold regions. More recently, Huerta et al. [19] coupled the PGD method with a domain decomposition technique to divide the solution process into two steps. In the first one, a PGD solution is obtained for each set of similar subdomains where these solutions are parametrized along the subdomains interfaces. In the second step, a global non-linear problem in the interfaces unknowns is solved. In this latter step, solution continuity and equilibrium are imposed in a weak sense. Bognet et al. [20] studied the response of composite plates under mechanical and thermal loads and highlighted the advantages in terms of computation time and resource saving when using a PGD approach. The possibility to perform parametric analyses by introducing extra-coordinates, besides the spatial ones, was also addressed. Later, the same approach was used for shell structures by Bognet et al. [21] and Chinesta et al. [22]. Authors stressed the fact the PGD-based approach is intrinsically different from plate and shell models as derived within the framework of classical structural mechanics such as, for instance, Kirchhoff-Love's, Reissner-Mindlin or Reddy's third-order theories, see Reddy [23]. A Matlab implementation of PGD for solid mechanics problems was presented by Cueto et al. [24]. Two-dimensional beams [25], plates [26,27] and cylindrical composite shells [28,29] were studied by Vidal and co-workers. A solution for composite plates with a hole, where the hole position is a solution space parameter was presented by Vidal et al. [30]. The solution space was enriched by considering the stacking sequence in composite plates by Vidal et al. [31]. Within the framework of Carrera's Unified Formulation [1], hierarchical PGD-based higher-order beam structural model were proposed by Polit et al. [32] and Giunta et al. [33]. Beams can be regarded as degenerated geometrical domains since they presented two characteristic dimensions (those identifying the cross-section) that are smaller than the axial extension and accurate solution by means of classical solution methods (such as mesh-based procedures), especially when composite materials are used, can become cumbersome, see Chinesta at al [34]. In this paper, in light of the interesting features of the variable separation, the PGD framework is applied to the study of composite beam structures. In the specific, fibre-reinforced laminated and sandwich three-dimensional beams with a generic cross-section geometry are investigated by means of a variable separation approach. The displacement field is approximated by a series of products of two coupled functions (also addressed as couples) that, respectively, depends upon the cross-section and axial coordinates only, as it is expressed in the beam theory approach. This particular choice allows us to consider any cross-section and derive refined models with layer wise capabilities. Each term in the series expansion consists in an enrichment of the solution approximation. A weak form formulation is, then, obtained by means of the principle of virtual works. One- and two-dimensional finite element approximations are assumed over the beam axis and cross-section, respectively. Over the cross-section, eight- and twelve-node serendipity shape function bases are considered. C^0 Lagrange interpolants are used along the axis. The original three-dimensional problem is divided into two coupled non-linear problems: a two-dimensional one over the cross-section and a one-dimensional problem over the axis. An iterative solution procedure is, then, adopted. Short and very short laminated and sandwich beams subjected to bending and both bending and torsion are investigated. Prismatic, box, z-shaped and longeron-type cross-sections are considered. Results are assessed toward literature solution or three-dimensional finite element solutions developed by a commercial software. The presented examples demonstrate that the proposed modeling approach yields solutions that are accurate yet computationally attractive.

2. Reference problem description: the governing equations

Let us consider a composite beam structure occupying the domain

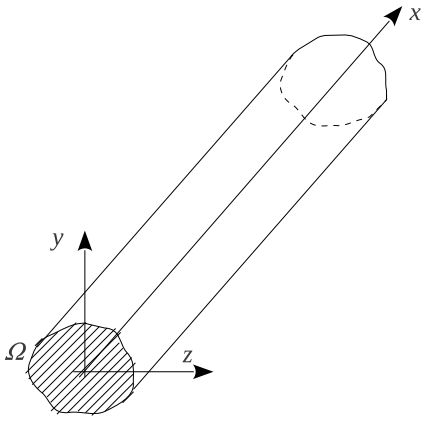

Fig. 1. Beam geometry and coordinate system.

$\mathscr{V} = \Omega \times \Omega_x$ where $\Omega_x = [0, L]$ (L being the length of the beam) and Ω is the cross-section in the (y, z) plane in a Cartesian coordinate (x, y, z). See Fig. 1.

2.1. Constitutive relation

The beam can be made of NC perfectly bonded orthotropic layers. The constitutive equations for a layer k can be written as

$$\boldsymbol{\sigma}^{(k)} = \mathbf{C}^{(k)}\boldsymbol{\varepsilon} \text{ for } (y, z) \in \Omega^{(k)} \tag{1}$$

where we denote the stress vector by $\boldsymbol{\sigma}$, the strain vector via $\boldsymbol{\varepsilon}$. $\Omega^{(k)}$ is the area (in the cross-section) of the layer k, $\Omega = \cup_{k=1}^{NC}\Omega^{(k)}$. We have

$$\mathbf{C}^{(k)} = \begin{bmatrix} C_{11}^{(k)} & C_{12}^{(k)} & C_{13}^{(k)} & 0 & 0 & C_{16}^{(k)} \\ & C_{22}^{(k)} & C_{23}^{(k)} & 0 & 0 & C_{26}^{(k)} \\ & & C_{33}^{(k)} & 0 & 0 & C_{36}^{(k)} \\ & & & C_{44}^{(k)} & C_{45}^{(k)} & 0 \\ & sym & & & C_{55}^{(k)} & 0 \\ & & & & & C_{66}^{(k)} \end{bmatrix} \tag{2}$$

where $C_{ij}^{(k)}$ are the three-dimensional stiffness coefficients of the layer (k). Note that this 3D constitutive law is used in the present formulation.

2.2. The weak form of the boundary value problem

The beam is submitted to a surface force density $\mathbf{t}$ defined over a subset Γ_N of the boundary and a body force density $\mathbf{b}$ defined in $\mathscr{V}$. We assume that a prescribed displacement $\mathbf{u} = \mathbf{u}_d$ is imposed on $\Gamma_D = \partial\mathscr{V} - \Gamma_N$.

Using the above matrix notations and for admissible displacement $\delta\mathbf{u} \in \delta U$, the variational principle is given by:

find $\mathbf{u} \in U$ such that:

$$-\int_{\mathscr{V}} \boldsymbol{\varepsilon}(\delta\mathbf{u})^T\boldsymbol{\sigma}\, d\mathscr{V} + \int_{\mathscr{V}} \delta\mathbf{u}^T\mathbf{b}\, d\mathscr{V} + \int_{\Gamma_N} \delta\mathbf{u}^T\mathbf{t}\, d\Gamma = 0$$
$$\forall\ \delta\mathbf{u} \in \delta U \tag{3}$$

where U is the space of admissible displacements, i.e. $U = \{\mathbf{u} \in (H^1(\mathscr{V}))^3 / \mathbf{u} = \mathbf{u}_d \text{ on } \Gamma_D\}$ and $\delta U = \{\mathbf{u} \in (H^1(\mathscr{V}))^3 / \mathbf{u} = 0 \text{ on } \Gamma_D\}$.

3. Application of the separated representation to the beam

In this section, we introduce the application of the variables separation for composite and sandwich beam analysis with any cross-sections. The idea consists in writing the displacement solution under a separated form involving 2D and 1D functions associated to the cross-

section ($\mathbf{v}^i(y,z)$, $i=1,2,3$) and the length of the beam ($\mathbf{f}^i(x)$, $i=1,2,3$), respectively. This approach differs from Ref. [25] by the choice of the separation as the present study allows us to consider any cross-section. The separated formulation is briefly introduced in the subsequent sections.

3.1. The displacement and the strain field

The displacement solution $\mathbf{u}$ is constructed as the sum of N products of separated functions ($N \in \mathbb{N}^+$ is the order of the representation)

$$\mathbf{u}(x,y,z) = \sum_{i=1}^{N} \mathbf{f}^i(x) \circ \mathbf{v}^i(y,z) \tag{4}$$

where $\mathbf{f}^i(x)$ and $\mathbf{v}^i(y,z)$ are unknown functions which must be computed during the resolution process. $\mathbf{f}^i(x)$ and $\mathbf{v}^i(y,z)$ are defined on Ω_x and Ω respectively. The "$\circ$" operator in Eq. (4) is Hadamard's element-wise product. We have:

$$\mathbf{f}^i \circ \mathbf{v}^i = \mathbf{v}^i \circ \mathbf{f}^i = \begin{bmatrix} f_1^i(x) v_1^i(y,z) \\ f_2^i(x) v_2^i(y,z) \\ f_3^i(x) v_3^i(y,z) \end{bmatrix} \quad \text{with } \mathbf{v}^i = \begin{bmatrix} v_1^i(y,z) \\ v_2^i(y,z) \\ v_3^i(y,z) \end{bmatrix} \mathbf{f}^i = \begin{bmatrix} f_1^i(x) \\ f_2^i(x) \\ f_3^i(x) \end{bmatrix} \tag{5}$$

The strain can be expressed with respect to the reference frame following

$$\varepsilon(u) = \sum_{i=1}^{N} \begin{bmatrix} (f_1^i)' v_1^i \\ f_2^i v_{2,2}^i \\ f_3^i v_{3,3}^i \\ f_2^i v_{2,3}^i + f_3^i v_{3,2}^i \\ f_1^i v_{1,3}^i + (f_3^i)' v_3^i \\ f_1^i v_{1,2}^i + (f_2^i)' v_2^i \end{bmatrix} \tag{6}$$

where the prime stands for the classical derivative ($f'_i = \frac{df_i}{dx}$), and for the partial derivative. The dependance with respect to the space coordinates is omitted.

3.2. Formulation of the problem to be solved

For sake of clarity, the body forces are neglected in the developments and the new problem to be solved is written as follows: find $\mathbf{u} \in \mathscr{U}$ ($U = \{\mathbf{u} \in (H^1(\mathscr{V}))^3 / \mathbf{u} = \mathbf{u}_d \text{ on } \Gamma_D\}$) such that

$$a(\mathbf{u}, \delta\mathbf{u}) = b(\delta\mathbf{u}) \;\forall\; \delta\mathbf{u} \in \delta\mathscr{U} \tag{7}$$

with

$$\begin{aligned} a(\mathbf{u}, \delta\mathbf{u}) &= \int_{\Omega_x \times \Omega} \varepsilon(\delta\mathbf{u})^T \mathbf{C} \varepsilon(\mathbf{u}) d\Omega d\Omega_x \\ b(\delta\mathbf{u}) &= \int_{\Gamma_N} \delta\mathbf{u}^T \mathbf{t}\, d\Gamma \end{aligned} \tag{8}$$

The expression of the strain, Eq. (6), introduced in the problem in Eq. (7) yields a non-linear parametrized problem that is solved by an iterative process. First, we assume that a sum of $m < N$ products of separated functions have been already computed. Therefore, the trial function for the iteration $m+1$ is written as

$$\mathbf{u}^{m+1}(x,y,z) = \mathbf{u}^m(x,y,z) + \mathbf{f}(x) \circ \mathbf{v}(y,z) \tag{9}$$

where $\mathbf{f}$ and $\mathbf{v}$ are the functions to be computed, and $\mathbf{u}^m$ is the associated known sets at iteration m defined by

$$\mathbf{u}^m(x,y,z) = \sum_{i=1}^{m} \mathbf{f}^i(x) \circ \mathbf{v}^i(y,z) \tag{10}$$

The problem to be solved given in Eq. (8) can be written as

$$a(\mathbf{f} \circ \mathbf{v}, \delta\mathbf{u}) = b(\delta\mathbf{u}) - a(\mathbf{u}^m, \delta\mathbf{u}) \tag{11}$$

The test function becomes

$$\delta(\mathbf{f} \circ \mathbf{v}) = \delta\mathbf{f} \circ \mathbf{v} + \mathbf{f} \circ \delta\mathbf{v} \tag{12}$$

Introducing the test function defined by Eq. (12) and the trial function defined by Eq. (9) into the weak form Eq. (11), the two following equations can be deduced:

- for the test function $\delta\mathbf{f}$

$$a(\mathbf{v} \circ \mathbf{f}, \mathbf{v} \circ \delta\mathbf{f}) = b(\mathbf{v} \circ \delta\mathbf{f}) - a(\mathbf{u}^m, \mathbf{v} \circ \delta\mathbf{f}) \quad \forall\; \delta\mathbf{f} \tag{13}$$

- for the test function $\delta\mathbf{v}$

$$a(\mathbf{f} \circ \mathbf{v}, \mathbf{f} \circ \delta\mathbf{v}) = b(\mathbf{f} \circ \delta\mathbf{v}) - a(\mathbf{u}^m, \mathbf{f} \circ \delta\mathbf{v}) \quad \forall\; \delta\mathbf{v} \tag{14}$$

from Eq. (13) and Eq. (14), a coupled non-linear problem is derived. A fixed point method is chosen to solve it. Starting from an initial function ($\tilde{\mathbf{f}}^{(0)}$, $\tilde{\mathbf{v}}^{(0)}$), we construct a sequence ($\tilde{\mathbf{f}}^{(l)}$, $\tilde{\mathbf{v}}^{(l)}$) which satisfy Eq. (13) and Eq. (14) respectively. For each problem, only one unknown 1D or 2D function has to be found, the other one is assumed to be known (from the previous step of the fixed point strategy). So, the approach leads to a classical iterative process which is not detailed here. Details can be found in Ref. [26]. The fixed point algorithm is stopped when the distance between two consecutive terms are sufficiently small.

3.3. Finite element discretization

To build the beam finite element approximation, a classical finite element approximation in Ω and Ω_x for ($\mathbf{v}$, $\mathbf{f}$) is introduced. The elementary vector of degrees of freedom (dof) associated with one element Ω_e of the mesh in Ω is denoted $\mathbf{q}_e^v$. The elementary vector of dofs associated with one element Ω_{x_e} of the mesh in Ω_x is denoted $\mathbf{q}_e^f$. The displacement fields and the strain field are determined from the values of $\mathbf{q}_e^v$ and $\mathbf{q}_e^f$ by

$$\begin{aligned} &\mathbf{v}_e = \mathbf{N}_{yz} \mathbf{q}_e^v, \quad \mathbf{E}_v^e = \mathbf{B}_{yz} \mathbf{q}_e^v, \\ &\mathbf{f}_e = \mathbf{N}_x \mathbf{q}_e^f, \quad \mathbf{E}_f^e = \mathbf{B}_x \mathbf{q}_e^f \end{aligned} \tag{15}$$

where

$$\mathbf{E}_v^{eT} = [v_1 \;\; v_{1,2} \;\; v_{1,3} \;\; v_2 \;\; v_{2,2} \;\; v_{2,3} \;\; v_3 \;\; v_{3,2} \;\; v_{3,3}]$$

$$\mathbf{E}_f^{eT} = [f_1 \;\; f_1' \;\; f_2 \;\; f_2' \;\; f_3 \;\; f_3']$$

The matrices $\mathbf{N}_{yz}$, $\mathbf{B}_{yz}$, $\mathbf{N}_x$, $\mathbf{B}_x$ contain the interpolation functions, their derivatives and the jacobian components.

3.4. Finite element problem to be solved on Ω

For the sake of simplicity, the functions $\tilde{\mathbf{f}}^{(l)}$ which are assumed to be known, will be denoted $\tilde{\mathbf{f}}$. And the function $\tilde{\mathbf{v}}^{(l)}$ to be computed will be denoted $\mathbf{v}$. The strains in Eq. (14) are defined as

$$\varepsilon(\tilde{f} \circ v) = \mathbf{\Sigma}_\mathbf{x}(\tilde{f}) \mathbf{E}_\mathbf{v} \tag{16}$$

with

$$\mathbf{\Sigma}_\mathbf{x}(\tilde{f}) = \begin{bmatrix} \tilde{f}_1' & 0 & 0 & 0 & 0 & 0 & 0 & 0 \\ 0 & 0 & 0 & 0 & \tilde{f}_2 & 0 & 0 & 0 & 0 \\ 0 & 0 & 0 & 0 & 0 & 0 & 0 & 0 & \tilde{f}_3 \\ 0 & 0 & 0 & 0 & 0 & \tilde{f}_2 & 0 & \tilde{f}_3 & 0 \\ 0 & 0 & \tilde{f}_1 & 0 & 0 & 0 & \tilde{f}_3' & 0 & 0 \\ 0 & \tilde{f}_1 & 0 & \tilde{f}_2' & 0 & 0 & 0 & 0 & 0 \end{bmatrix} \tag{17}$$

The variational problem defined on Ω from Eq. (14) is

$$\sum_{k=1}^{NC} \int_{\Omega^{(k)}} [\delta \mathbf{E}_{\mathbf{v}}^T \mathbf{k}_x^k(\tilde{f}) \mathbf{E}_{\mathbf{v}}] d\Omega^k$$
$$= \int_{\Omega_N} \delta \mathbf{v}^T \mathbf{t}_x(\tilde{f}) d\Omega_N - \sum_{k=1}^{NC} \int_{\Omega^{(k)}} [\delta \mathbf{E}_{\mathbf{v}}^T \boldsymbol{\sigma}_x^k(\tilde{f}, \mathbf{u}^m)] d\Omega^k \tag{18}$$

where

$$\mathbf{k}_x^k(\tilde{f}) = \int_{\Omega_x} \boldsymbol{\Sigma}_{\mathbf{x}}(\tilde{f})^T \mathbf{C}^k \boldsymbol{\Sigma}_{\mathbf{x}}(\tilde{f}) dx \tag{19}$$

and

$$\mathbf{t}_x(\tilde{f}) = \int_{\Omega_x} \tilde{\mathbf{f}} \circ \mathbf{t} dx$$
$$\boldsymbol{\sigma}_x^k(\tilde{f}, \mathbf{u}^m) = \int_{\Omega_x} [\boldsymbol{\Sigma}_{\mathbf{x}}(\tilde{f})^T \mathbf{C}^k \boldsymbol{\varepsilon}(\mathbf{u}^m)] dx \tag{20}$$

Ω_N is the 1D domain of the cross-section where the load is applied.

Remark. In Eq. (18), the different integrations over $\Omega^{(k)}$ should be gathered in *NbMat* areas that have the same orthotropic characteristics (the layers with the same ply orientation).

The introduction of the finite element approximation Eq. (15) in the variational Eq. (18) leads to the linear system

$$\mathbf{K}_x(\tilde{f}) \mathbf{q}^v = \mathbf{R}_t(\tilde{f}) - \mathbf{R}_v(\tilde{f}, \mathbf{u}^m) \tag{21}$$

where

- $\mathbf{q}^v$ is the vector of the nodal displacements, associated with the finite element mesh in Ω,
- $\mathbf{K}_x(\tilde{f})$ is the mechanical stiffness matrix obtained by summing the elements' stiffness matrices $\mathbf{K}_x^e(\tilde{f}) = \int_{\Omega_e} [\mathbf{B}_{yz}^T \mathbf{k}_x^k(\tilde{f}) \mathbf{B}_{yz}] d\Omega_e$
- $\mathbf{R}_t(\tilde{f}) - \mathbf{R}_v(\tilde{f}, \mathbf{u}^m)$ is the equilibrium mechanical residual obtained by summing the elements' load vectors $\int_{\Omega_{Ne}} \mathbf{N}_{yz}^T \mathbf{t}_z(\tilde{f}) d\Omega_{Ne}$ and $\int_{\Omega_e} \mathbf{B}_{yz}^T \boldsymbol{\sigma}_x^k(\tilde{f}, \mathbf{u}^m) d\Omega_e$ (associated to the known terms)

3.5. Finite element problem to be solved on Ω_x

As in the previous section, the known functions $\tilde{\mathbf{v}}^{(l-1)}$ will be denoted $\tilde{\mathbf{v}}$ and the functions $\tilde{\mathbf{f}}^{(l)}$ to be computed will be denoted $\mathbf{f}$. The strain in Eq. (13) is defined as

$$\boldsymbol{\varepsilon}(\tilde{v} \circ f) = \boldsymbol{\Sigma}_{\mathbf{yz}}(\tilde{v}) \mathbf{E}_{\mathbf{f}} \tag{22}$$

where

$$\boldsymbol{\Sigma}_{\mathbf{yz}}(\tilde{v}) = \begin{bmatrix} 0 & \tilde{v}_1 & 0 & 0 & 0 & 0 \\ 0 & 0 & \tilde{v}_{2,2} & 0 & 0 & 0 \\ 0 & 0 & 0 & 0 & \tilde{v}_{3,3} & 0 \\ 0 & 0 & \tilde{v}_{2,3} & 0 & \tilde{v}_{3,2} & 0 \\ \tilde{v}_{1,3} & 0 & 0 & 0 & 0 & \tilde{v}_3 \\ \tilde{v}_{1,2} & 0 & 0 & \tilde{v}_2 & 0 & 0 \end{bmatrix} \tag{23}$$

The variational problem defined on Ω_x from Eq. (13) is

$$\int_{\Omega_x} \delta \mathbf{E}_{\mathbf{f}}^T \mathbf{k}_{yz}(\tilde{v}) \mathbf{E}_{\mathbf{f}} dx$$
$$= \int_{\Omega_x} \delta \mathbf{f}^T \mathbf{t}_{yz}(\tilde{v}) dx - \int_{\Omega_x} \delta \mathbf{E}_{\mathbf{f}}^T \boldsymbol{\sigma}_{yz}(\tilde{v}, \mathbf{u}^m) dx \tag{24}$$

where $\mathbf{k}_{yz}(\tilde{v})$ can be expressed under the following separated form:

$$\mathbf{k}_{yz}(\tilde{v}) = \int_{\Omega} \boldsymbol{\Sigma}_{\mathbf{yz}}(\tilde{v})^T \mathbf{C} \boldsymbol{\Sigma}_{\mathbf{yz}}(\tilde{v}) d\Omega \tag{25}$$

We also define:

$$\mathbf{t}_{yz}(\tilde{v}) = \int_{\Omega_N} \tilde{\mathbf{v}} \circ \mathbf{t} d\Omega_N$$
$$\boldsymbol{\sigma}_{yz}(\tilde{v}, \mathbf{u}^m) = \int_{\Omega} [\boldsymbol{\Sigma}_{\mathbf{yz}}(\tilde{v})^T (\mathbf{C} \boldsymbol{\varepsilon}(\mathbf{u}^m))] d\Omega \tag{26}$$

The introduction of the finite element discretization Eq. (15) in the variational Eq. (24) leads to the linear system

$$\mathbf{K}_{yz}(\tilde{v}) \mathbf{q}^f = \mathbf{R}_{ft}(\tilde{v}) - \mathbf{R}_{fv}(\tilde{v}, \mathbf{u}^m) \tag{27}$$

where

- $\mathbf{q}^f$ is the vector of degree of freedom associated with the F.E. approximations in Ω_x.
- $\mathbf{K}_{yz}(\tilde{v})$ is obtained by summing the elements' stiffness matrices:

$$\mathbf{K}_{yz}^e(\tilde{v}) = \int_{\Omega_{xe}} [\mathbf{B}_x^T \mathbf{k}_{yz}(\tilde{v}) \mathbf{B}_x] dx_e \tag{28}$$

- $\mathbf{R}_{ft}(\tilde{v}) - \mathbf{R}_{fv}(\tilde{v}, \mathbf{u}^m)$ is an equilibrium residual, it is obtained by the summation of the elements' residual vectors coming from the right hand side of Eq. (24).

4. Numerical results

In this section, the present approach is assessed through various static test cases with both laminated and sandwich beams. Different types of cross-section (square, box, Z-shaped) are also considered to illustrate the performance of the method. Finally, a composite type-longeron is addressed.

In the subsequent sections, results can be compared with

- a three-dimensional FEM solution obtained via the commercial code Ansys. The 20-node solid element SOLID186 is used. Unless otherwise stated, the same cross-section mesh is used to generate the 3D mesh,
- an exact elasticity solution from Ref. [35].

The F.E. discretization of the 2D problem associated to the cross-section is based on a classical Serendipity interpolation functions involving eight (Fig. 2(a)) or twelve (Fig. 2(b)) nodes per element. The 1D FE problem is discretized with classical lagrange interpolations. A mesh with $N_x = 8$ elements is sufficient and will be used in all numerical tests.

4.1. Pagano test case with a square cross-section

To see the capability of the present approach to model laminated composite beam, an antisymmetric beam is addressed as in Ref. [35]. It is detailed below:

geometry: composite cross-ply beam [0°/90°] ($NC = 2$) and length-to-thickness ratio S = L/h = 4. All layers have the same thickness.
geometry of the cross-section: symmetric square cross-section
boundary conditions: simply supported beam subjected to sinusoidal load $q(x) = q_0 \sin\frac{\pi x}{L}$.
material properties: $E_L = 25\text{GPa}$, $E_T = 1\text{GPa}$, $G_{LT} = 0.5\text{GPa}$, $G_{TT} = 0.2\text{GPa}$, $\nu_{LT} = \nu_{TT} = 0.25$
where L refers to the fiber direction, T refers to the transverse direction.

2D cross-section mesh: the number of elements along the y and z-

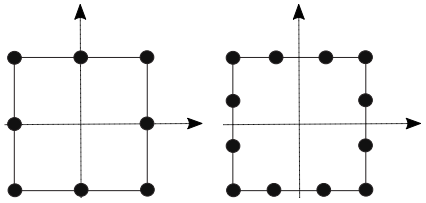

Fig. 2. Serendipity finite elements.

Table 1
Convergence study - two layers (0°/90°) - VS-Q8 - sinusoidal pressure.

α_{layer}		$\bar{u}(h/2)$	$\bar{w}(0)$	$\bar{\sigma}_{11}(-h/2)$	$\bar{\sigma}_{13max}$	$\bar{\sigma}_{33}(h/2)$
1		−4.3388	4.5073	−27.6933	2.4164	1.0565
	Error	5.02%	4.25%	7.75%	11.17%	5.65%
2		−4.5468	4.6863	−29.8866	3.1021	1.0175
	Error	0.46%	0.45%	0.44%	14.03%	1.75%
3		−4.5608	4.6984	−30.0228	2.7885	1.0104
	Error	0.16%	0.19%	0.01%	2.50%	1.04%
4		−4.5632	4.7006	−30.0430	2.7873	1.0038
	Error	0.11%	0.15%	0.08%	2.46%	0.38%
6		−4.5644	4.7015	−30.0473	2.7383	0.9967
	Error	0.08%	0.13%	0.09%	0.66%	0.33%
	Exact	−4.5680	4.7076	−30.0197	2.7204	1.0000

axis is $\alpha_{layer}NC$, where α_{layer} is the number of elements per layer along the z-axis.

number of dofs (2D problem): $Ndof_{yz} = 3(3\alpha_{layer}NC+1)(\alpha_{layer}NC+1)$ for Q8; $Ndof_{yz} = 3(5\alpha_{layer}NC+1)(\alpha_{layer}NC+1)$ for Q12

results: The results ($\bar{u}$, $\bar{w}$, $\bar{\sigma}_{11}$, $\bar{\sigma}_{13}$) are made non-dimensional using:

$$\bar{u} = u_1(0,0,h/2)\frac{E_T}{hq_0}\ \bar{w} = u_3(L/2,0,0)\frac{100E_T}{S^4hq_0}$$
$$\bar{\sigma}_{ij} = \sigma_{ij}\frac{1}{q_0}\ \text{for}\ \begin{cases}\sigma_{11}(L/2,0,h/2)\\ \sigma_{13}(0,0,0)\end{cases} \tag{29}$$

They are compared with exact elasticity solution [35].

The present approach is assessed on a two-layer beam as this configuration is a challenging test case for the refined beam model. The aim of the study consists in showing the influence of the order of cross-section elements on the accuracy of the results. Thus, a convergence study is addressed using either $Q8$ (denoted VS-Q8) or $Q12$ (denoted VS-Q12) elements. The results are summarized in Table 1 and Table 2. They show the superiority of the Q12 element: the convergence is very high for both displacements and stresses, and only 2 elements per layer are needed to obtain an error rate of less than 0.55%. Due to the order expansion of Q8 element, the distribution of the transverse shear stress along the thickness is linear in each element, and at least 6 elements per layer is required to have a low error rate. The distribution of $\bar{\sigma}_{13}$ is given in Fig. 3 for different values of α_{layer}. The asymetrical distribution of $\bar{\sigma}_{13}$ is in excellent agreement with the exact solution using a coarse Q12 mesh. The top and bottom boundary conditions and the continuity at the interface layers are fulfilled.

4.2. Sandwich beam with a square cross-section

A sandwich beam with two different materials [36] is investigated with the following characteristics:

geometry: 3-layer sandwich beam with thickness 0.001 m (face)/ 0.01 m (core)/0.001 m (face) and length-to-thickness ratio S = 5 and 10; half of the beam is meshed,

geometry of the cross-section: symmetric square cross-section ($b \times h$, being b the width)

boundary conditions: simply supported beam under a sinusoidal pressure $q(x) = q_0\sin\frac{\pi x}{L}$

material properties: Two material configurations are considered:

- Type I: the face sheets and the core are made of aluminium.
  Face: $E_f^I = 69000$MPa, $\nu_f^I = 0.33$.
  Core: hexagonal cells with the following equivalent properties, $E_{c1}^I = E_{c2}^I = 1.62$MPa, $E_{c3}^I = 2.3$GPa, $\nu_{c12}^I = 0.99$, $\nu_{c13}^I = \nu_{c23}^I = 2.3210^{-4}$, $G_{c12}^I = 0.97$MPa, $G_{c13}^I = 499$MPa, $G_{c23}^I = 324$MPa
- Type II: the skins are made of T300/5208 graphite/epoxy with fibres aligned along the beam axis.
  Face: $E_{f1}^{II} = 135.5$GPa, $E_{f2}^{II} = E_{f3}^{II} = 10.8$GPa, $\nu_{f12}^{II} = \nu_{f13}^{II} = 0.24$, $\nu_{f23}^{II} = 0.49$, $G_{f12}^{II} = G_{f13}^{II} = 5.7$GPa, $G_{f23}^{II} = 3.4$GPa
  Core made of Nomex: $E_{c1}^{II} = 0.10$MPa, $E_{c2}^{II} = 0.11$MPa, $E_{c3}^{II} = 109$MPa, $\nu_{c12}^{II} = 0.9$, $\nu_{c13}^{II} = \nu_{f23}^{II} = 210^{-4}$, $G_{c12}^{II} = 0.1$MPa, $G_{c13}^{II} = 25$MPa, $G_{c23}^{II} = 18$MPa

2D cross-section mesh: the number of elements along the z-axis is $2N_{face} + N_{core}$, where N_{face} and N_{core} are the number of elements in the face and in the core, respectively.

number of dofs (2D problem): $Ndof_{yz} = 3(3(2N_{face} + N_{core}) + 1)(2N_{face} + N_{core} + 1)$ for Q8; $Ndof_{yz} = 3(5(2N_{face} + N_{core}) + 1)(2N_{face} + N_{core} + 1)$ for Q12

results: the following displacements and stresses are assessed:

$$\hat{u}_1 = u_1(0, b/2, -h/2),\ \hat{u}_2 = u_2(L/2, b/2, -h/2),\ \hat{u}_3 = u_3(L/2, b/2, h/2),$$
$$\hat{\sigma}_{11} = \sigma_{11}(L/2, b/2, h/2),\ \hat{\sigma}_{22} = \sigma_{22}(L/2,0, h/2),\ \hat{\sigma}_{13} = \sigma_{13}(0,0,0)$$
$$\hat{\sigma}_{13max} = \max(\sigma_{13}(0,0, z)) \tag{30}$$

Results are compared with a 3D FEM solution. The same number of elements along cross-section width and thickness is used. The total number of degrees of freedom of the three-dimensional FEM solution as function of n_{3D} (number of elements over the cross-section) and n_{x3D} (number of elements over half of the axial span) are: . Considering n_{x3D} =8 as for the PGD results and n_{3D} = 48 (8 and 32 elements along the faces and core thickness, respectively), we obtain the number of dofs equal to 247131.

Note that the second configuration (type II) presents a higher difference between skins and core material properties and, therefore, it is more challenging from a modeling point of view. For this test, only one couple is built to obtain the solution. First of all, a convergence study for the cross-section 2D mesh is carried out for this second configuration for both Q8 and Q12 elements. The results are given in Table 3 and Table 4, varying the number of elements along the z-axis in the face (N_{face}) and in the core (N_{core}). We can notice that the convergence rate of the displacements are very high for the two types of element. A 1/4 mesh yields a very accurate results. Nevertheless, as previously, the transverse shear stress requires the use of a more refined mesh. A 2/8 one is sufficient to obtain an error rate of 0.8% for Q12 whereas an 8/32 one is required using Q8 elements. Moreover, the comparison in terms of number of dofs for the most costly problem (2D one) shows clearly the advantage to use higher-order FE for the modeling of sandwich structures (2379 dofs for Q12 vs 21315 for Q8). As far as the comparison with the 3D FEM cost is concerned, the present approach allows us to reduce the computational cost. Even if the number of dofs of the 2D problem of the present method is just an indicator, this one is divided by about one hundred with respect to the 3D approach in this example.

Then, the present approach using Q12 elements is assessed for a thick (S = 5) and a moderately thick (S = 10) beam for the two types of material. The results are summarized in Table 5 and Table 6. The displacements and the stresses are in excellent agreement with the reference solution. For further assessment, the distributions of the displacements and stresses though the thickness are given in Figs. 4 and 5

Table 2
Convergence study - two layers (0°/90°) - VS-Q12 - sinusoidal pressure.

α_{layer}		$\bar{u}(h/2)$	$\bar{w}(0)$	$\bar{\sigma}_{11}(-h/2)$	$\bar{\sigma}_{13max}$	$\bar{\sigma}_{33}(h/2)$
1		−4.5760	4.7120	−30.1917	2.7750	1.0292
	error	0.17%	0.09%	0.57%	2.01%	2.92%
2		−4.5648	4.7017	−30.0540	2.7140	0.9945
	error	0.07%	0.13%	0.11%	0.24%	0.55%
3		−4.5644	4.7017	−30.0446	2.7198	1.0152
	error	0.08%	0.13%	0.08%	0.02%	1.52%
4		−4.5648	4.7017	−30.0414	2.7174	1.0103
	error	0.07%	0.13%	0.07%	0.11%	1.03%
6		−4.5648	4.7017	−30.0452	2.7177	1.0086
	error	0.07%	0.12%	0.08%	0.10%	0.86%
	exact	−4.5680	4.7076	−30.0197	2.7204	1.0000

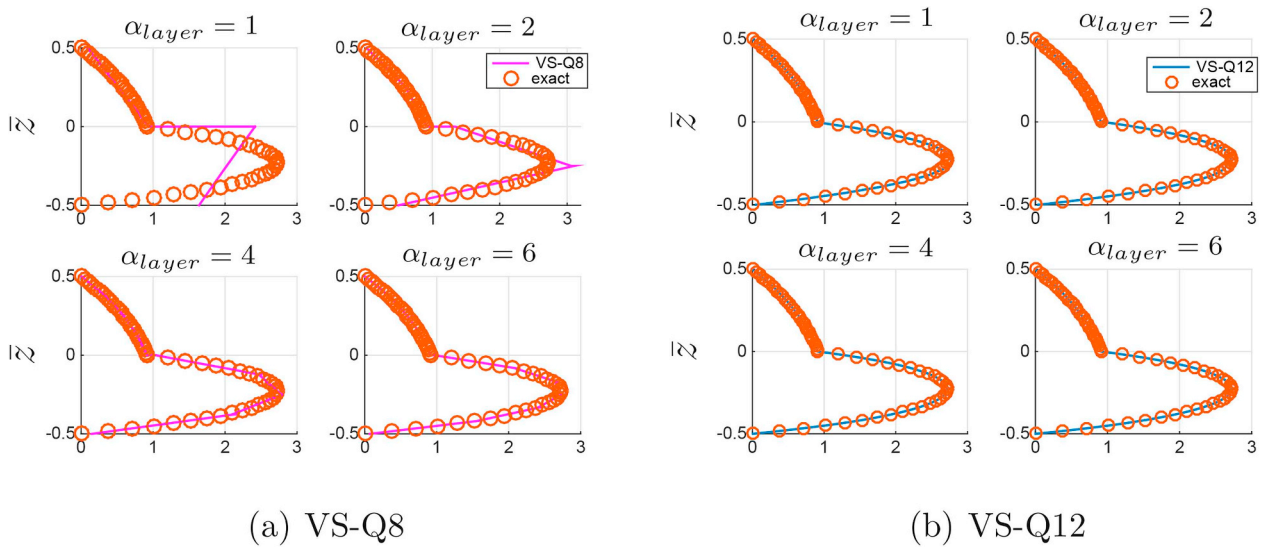

Fig. 3. Distribution of $\bar{\sigma}_{13}$ along the thickness - S = 4 - 2 layers - [0°/90°] - sinusoidal pressure.

Table 3
Convergence study VS-Q8 - sandwich beam - type II - S = 5.

N_{face}/N_{core}	$Ndof_{yz}$		$\hat{u}_1$	$\hat{u}_2$	$\hat{u}_3$	$\hat{\sigma}_{11}$	$\hat{\sigma}_{22}$	$\hat{\sigma}_{13}$	$\hat{\sigma}_{13max}$
1/4	399		2.5323e-11	1.4084e-12	7.7333e-10	2.2513e+02	2.0068e+00	1.3027e+00	3.3882e+00
		error	0.01%	0.41%	0.00%	0.01%	1.98%	0.01%	12.00%
2/8	1443		2.5330e-11	1.4141e-12	7.7362e-10	2.2514e+02	1.9921e+00	1.3029e+00	4.3389e+00
		error	0.03%	0.01%	0.03%	0.00%	1.23%	0.01%	12.69%
4/16	5475		2.5330e-11	1.4148e-12	7.7364e-10	2.2515e+02	1.9753e+00	1.3029e+00	3.9471e+00
		error	0.03%	0.04%	0.04%	0.00%	0.38%	0.01%	2.52%
8/32	21315		2.5330e-11	1.4147e-12	7.7364e-10	2.2516e+02	1.9697e+00	1.3028e+00	3.8495e+00
		error	0.03%	0.03%	0.04%	0.01%	0.09%	0.00%	0.02%
Ref.			2.5321e-11	1.4142e-12	7.7337e-10	2.2514e+02	1.9679e+00	1.3028e+00	3.8501e+00

Table 4
Convergence study VS-Q12 - sandwich beam - type II - S = 5.

N_{face}/N_{core}	$Ndof_{yz}$		$\hat{u}_1$	$\hat{u}_2$	$\hat{u}_3$	$\hat{\sigma}_{11}$	$\hat{\sigma}_{22}$	$\hat{\sigma}_{13}$	$\hat{\sigma}_{13max}$
1/4	651		2.5328e-11	1.4139e-12	7.7364e-10	2.2517e+02	1.9866e+00	1.3028e+00	1.3066e+00
		error	0.03%	0.02%	0.04%	0.01%	0.95%	0.00%	66.06%
2/8	2379		2.5329e-11	1.4147e-12	7.7364e-10	2.2515e+02	1.9693e+00	1.3028e+00	3.8165e+00
		error	0.03%	0.03%	0.04%	0.00%	0.07%	0.00%	0.87%
4/16	9075		2.5330e-11	1.4148e-12	7.7364e-10	2.2515e+02	1.9678e+00	1.3028e+00	3.8169e+00
		error	0.03%	0.04%	0.04%	0.00%	0.01%	0.00%	0.86%
Ref.			2.5321e-11	1.4142e-12	7.7337e-10	2.2514e+02	1.9679e+00	1.3028e+00	3.8501e+00

for the more challenging test. The approach performs very well when compared to the 3D results. A zig-zag behavior occurs for the in-plane displacements. The variation of u_2 and u_3 though the core is not linear. For this thick case, we also notice that the distribution of σ_{13} is complex with a localised effect in the faces (Fig. 5 (right)). Thus, the present separated representation has the capability to model a wide range of sandwich structures.

4.3. Box cross-section beam

A box cross-section beam submitted to an off-centric pressure load is considered in order to investigate a problem where both bending and torsion are involved. Moreover, the presence of sharp corners in the cross-section makes the prediction of mechanical response not trivial. The test case is described below:

Table 5
Sandwich beam - type I – VS-Q12.

S		$\hat{u}_1$	$\hat{u}_2$	$\hat{u}_3$	$\hat{\sigma}_{11}$	$\hat{\sigma}_{22}$	$\hat{\sigma}_{13}$
5		8.5811e-12	8.2602e-13	7.3466e-11	3.7349e+01	1.9567e+00	1.7351e+00
	error	0.04%	0.03%	0.04%	0.04%	0.15%	0.00%
	Ref.	8.5780e-12	8.2573e-13	7.3440e-11	3.7365e+01	1.9537e+00	1.7350e+00
10		6.0286e-11	3.0556e-12	5.6564e-10	1.3065e+02	1.9215e+00	3.4979e+00
	error	0.04%	0.04%	0.04%	0.02%	0.14%	0.00%
	Ref.	6.0265e-11	3.0545e-12	5.6543e-10	1.3067e+02	1.9188e+00	3.4979e+00

Table 6

Sandwich beam - type II – VS-Q12.

S		$\hat{u}_1$	$\hat{u}_2$	$\hat{u}_3$	$\hat{\sigma}_{11}$	$\hat{\sigma}_{22}$	$\hat{\sigma}_{13}$
5		2.5330e-11	1.4148e-12	7.7364e-10	2.2515e+02	1.9753e+00	1.3029e+00
	error	0.04%	0.04%	0.04%	0.03%	0.31%	0.01%
	Ref.	2.5321e-11	1.4142e-12	7.7337e-10	2.2514e+02	1.9679e+00	1.3028e+00
10		8.4100e-11	2.5881e-12	3.8664e-09	3.6037e+02	2.2603e+00	3.2370e+00
	error	0.04%	0.04%	0.04%	0.01%	0.22%	0.00%
	Ref.	8.4069e-11	2.5872e-12	3.8650e-09	3.6035e+02	2.2553e+00	3.2370e+00

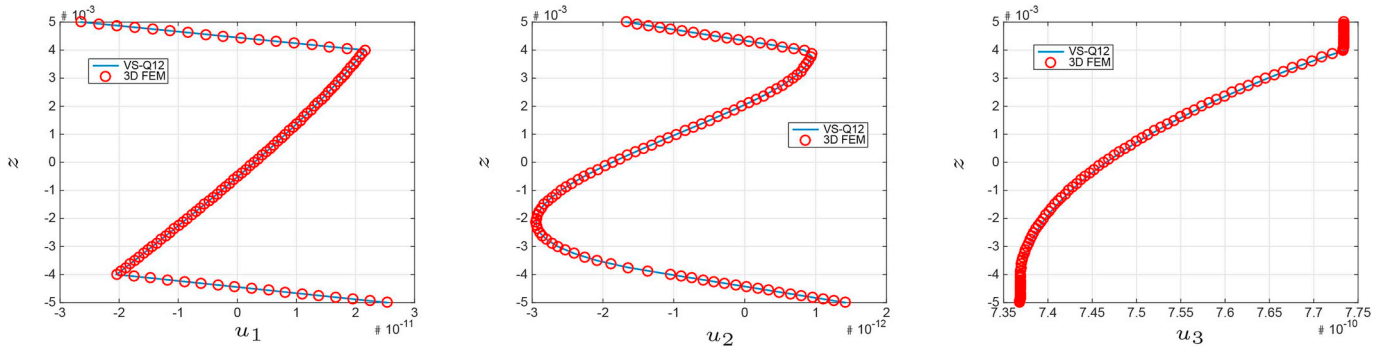

Fig. 4. $u_1(0, h/2, z)$ (left), $u_2(L/2, h/2, z)$ (middle), $u_3(L/2, h/2, z)$ (right) - sandwich beam - type II.

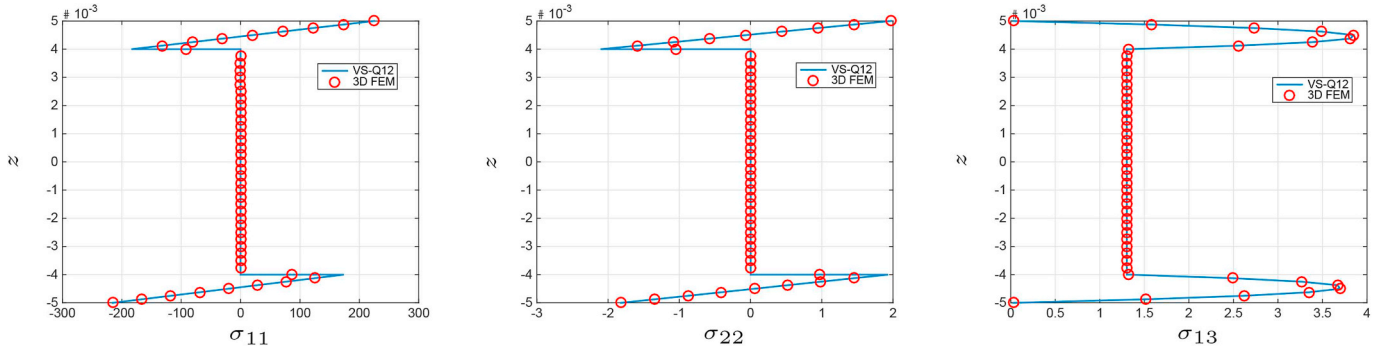

Fig. 5. $\sigma_{11}(L/2, h/2, z)$ (left), $\sigma_{22}(L/2{,}0, z)$ (middle), $\sigma_{13}(0{,}0, z)$ (right) - sandwich beam - type II.

geometry: a [0°/90°] box cross-section beam with the thickness of each layer equal to $a/10$ and $S = 4$
geometry of the cross-section: box square cross-section
boundary conditions: simply supported beam $(u_3(0, y, z) = u_3(L, y, z) = 0)$ subjected to an off-centric pressure load p_{zz} as illustrated in Fig. 6
material properties: same material as in Section 4.1
2D cross-section mesh: cf. Fig. 6 (right)
results: Displacements and stresses are put into the following dimensionless form:

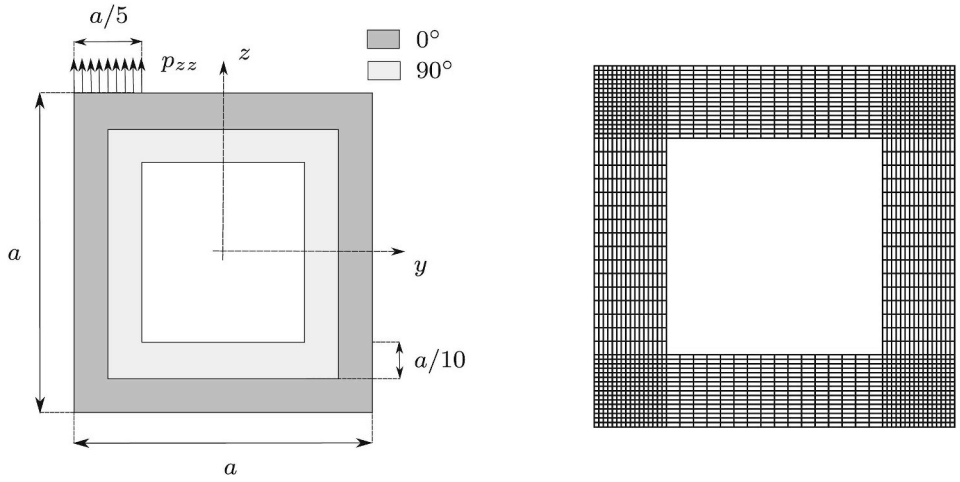

Fig. 6. Box cross-section (left) - 2D mesh (right).

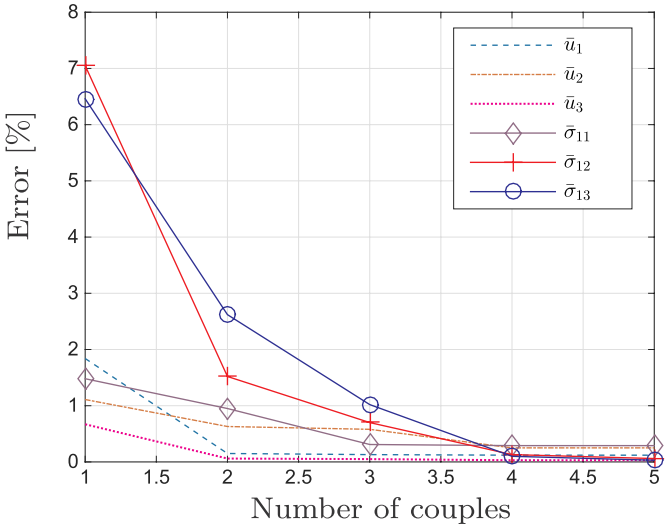

Fig. 7. Error with respect to the number of couples - [0°/90°] Box cross-section.

Table 7
Two layers [0°/90°] Box cross-section.

model	$\bar{u}_1$	$\bar{u}_2$	$\bar{u}_3$	$\bar{\sigma}_{11}$	$\bar{\sigma}_{12}$	$\bar{\sigma}_{13}$
VS-Beam	4.106	9.006	0.449	24.24	2.350	5.114
error	0.12%	0.25%	0.03%	0.29%	0.06%	0.03%
3D FEM	4.111	8.983	0.449	24.31	2.349	5.113

$$\bar{u}_i = \frac{E_T}{p_{zz}a}u_i \text{ with } i = 1,2 \quad \bar{u}_3 = 100\frac{E_T a^3}{p_{zz}L^4}u_3 \text{ for } \begin{cases} u_1(0, -a/2, -a/2) \\ u_2(L/2, -a/2, -a/2) \\ u_3(L/2, -a/2, -a/2) \end{cases}$$

$$\bar{\sigma}_{ij} = \frac{1}{p_{zz}}\sigma_{ij} \text{ for } \begin{cases} \sigma_{11}(L/2,0, a/2) \\ \sigma_{13}(0, -a/2,0) \\ \sigma_{12}(0,0, -a/2) \end{cases} \tag{31}$$

Present VS-Beam results are compared with a 3D FEM solution computed by the commercial code Ansys.

First, a convergence rate with respect to the number of couples is provided in Fig. 7. Only one couple allows us to have a good estimation of the displacements. Five couples are needed to obtain an accurate result for stresses.

Table 7 presents the dimensionless displacements $\bar{u}_i$ and stresses $\bar{\sigma}_{11}$, $\bar{\sigma}_{12}$ and $\bar{\sigma}_{13}$. The agreement with the 3D solution is very good. The variations over the cross-section of displacements and stresses are also shown in Figs. 8–12. Results agree very well for the displacements and the stress components. In the case of the shear stresses, the internal sharp corner in the cross-section give rise to stress concentrations that make the solution difficult to be accurately predicted. We can notice that this localised effect is successfully captured by the present approach where the cross-section is discretized by 2D quadrilateral elements. This approach overcomes the limitations highlighted in Ref. [32] where MacLaurin's polynomials are used for the y-z functions.

4.4. Z-shaped beam

A beam cross-section with reentrant corners (Z-shaped cross-section) is considered. Both bending and torsion are involved in this example. The test case is described as follows:

geometry: a [0°/90°] beam with $S = 4$, all layers have the same

(a) VS-Q12 (b) 3D Ansys

Fig. 8. $\bar{u}_1(x = 0, y, z)$ - [0°/90°] Box cross-section.

(a) VS-Q12 (b) 3D Ansys

Fig. 9. $\bar{u}_3(x = L/2, y, z)$ - [0°/90°] Box cross-section.

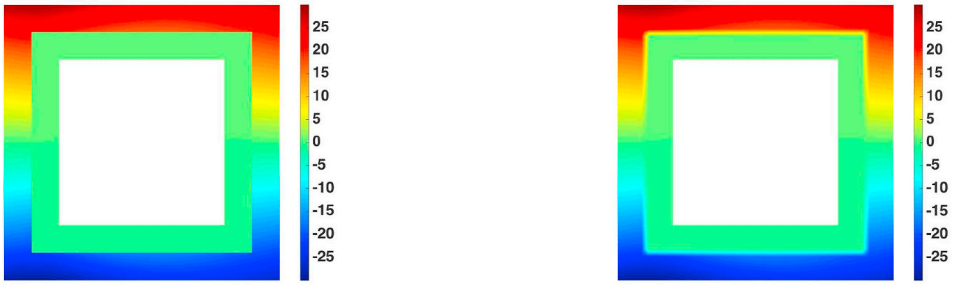

Fig. 10. $\bar{\sigma}_{11}(x = L/2, y, z)$ - [0°/90°] Box cross-section.

Fig. 11. $\bar{\sigma}_{12}(x = 0, y, z)$ - [0°/90°] Box cross-section.

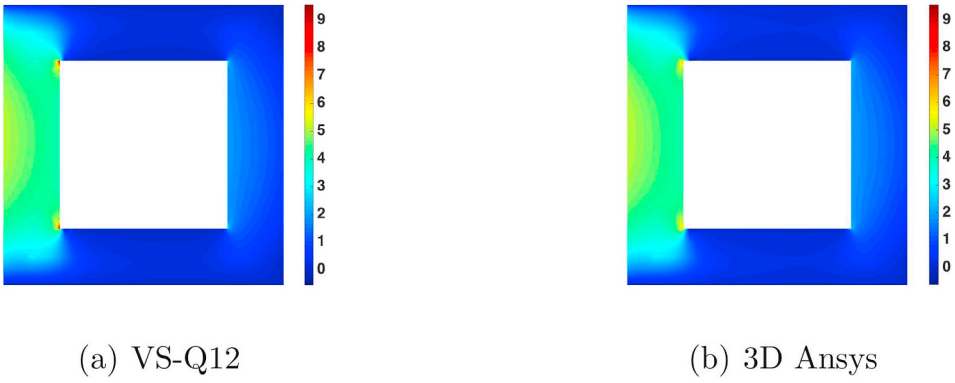

Fig. 12. $\bar{\sigma}_{13}(x = 0, y, z)$ - [0°/90°] Box cross-section.

thickness.

geometry of the cross-section: Z-shaped cross-section as illustrated in Fig. 13 with $ep_a = 7.10^{-2}$ m, $ep_b = 4.10^{-2}$ m and $ep_t = 3.10^{-2}$ m

boundary conditions: simply supported beam ($u_3(0, y, z) = u_3(L, y, z) = 0$) subjected to a constant pressure load p_z at the top of the beam

material properties: same material as in Section 4.1

2D cross-section mesh: cf. Fig. 13 (right)

results: Displacements and stresses cross-section are given. 3D FEM solution is used as reference one.

5 couples ensure coincident results between the present approach (VS-Beam) and the 3D FEM solution. Figs. 14–18 give the distributions of displacements and stresses over the cross-section. Classical beam models fail to model such configurations. In fact, distributions of displacements along the thickness or the width are not simple. A singularity occurs in a corner of the cross-section for the transverse shear stresses (cf. Fig. 17 and 18). It is well captured by the present approach. Despite these difficulties, excellent results are obtained when compared to the 3D reference solution over the cross-section. In Fig. 19, the good accuracy of the transverse shear stresses is confirmed at different locations of the cross-section. An inhomogeneous stress state can be clearly seen.

4.5. Composite-type longeron

In this section, the presented test case aims at analyzing a typical simplified longeron structure for aerospace applications. It is proposed in Ref. [37]. A beam made of composite materials, assembled with different parts, is considered. The characteristics are given below:

geometry: a composite beam with $L = 1$ m,

geometry of the cross-section: Longeron type cross-section as

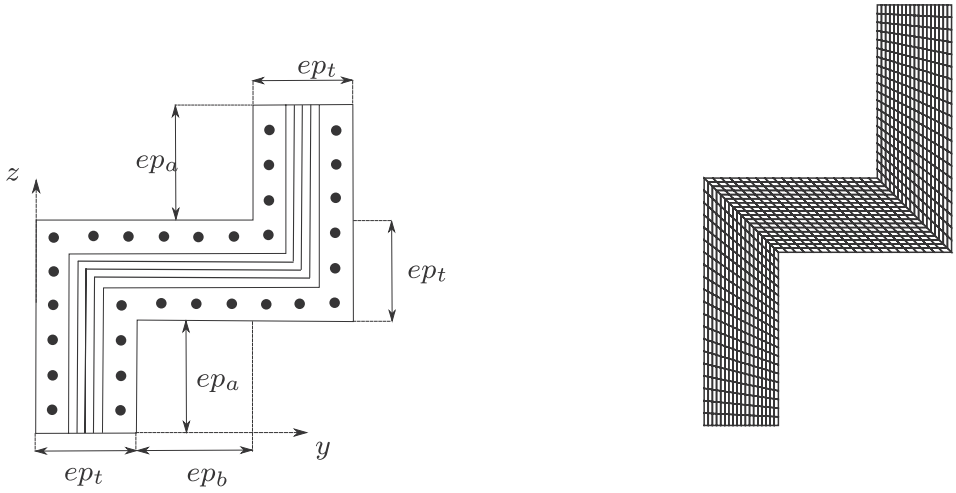

Fig. 13. Z-shaped beam (left) - 2D mesh (right).

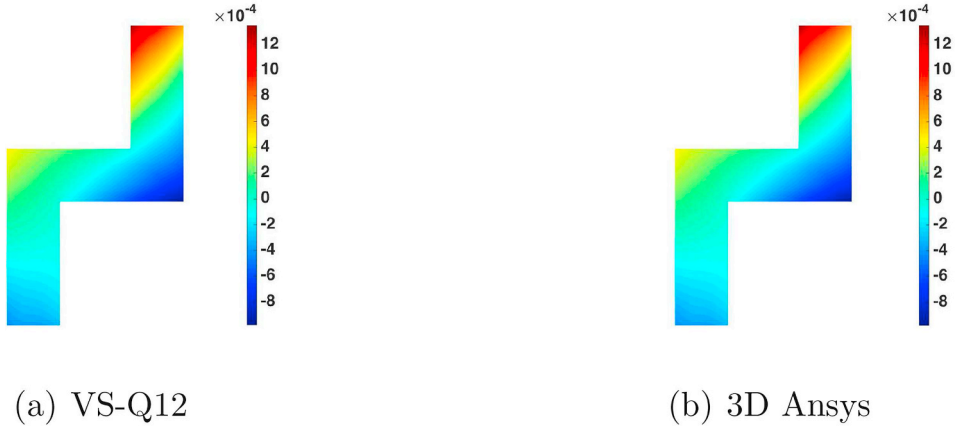

Fig. 14. $u_1(x = 0, y, z)$ - Z-shaped beam.

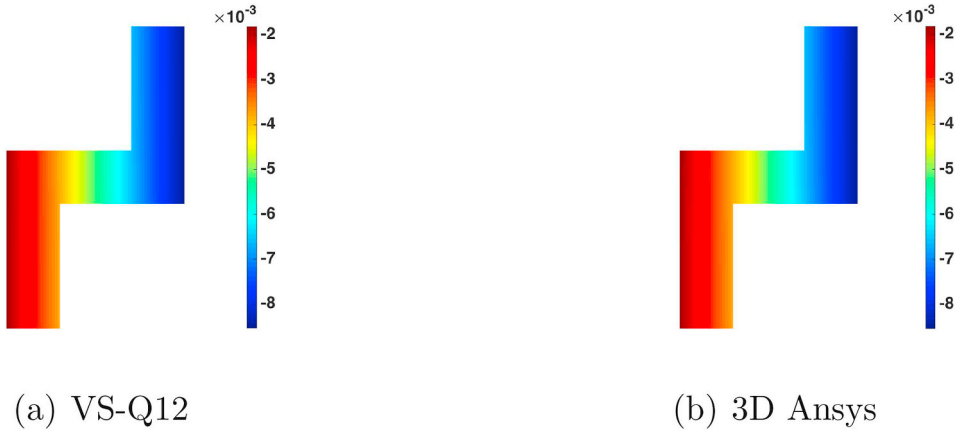

Fig. 15. $u_3(x = L/2, y, z)$ - Z-shaped beam.

illustrated in Fig. 20 (left) with $a = 0.1$ m, $b = 0.044$ m, $c = 0.04$ m, $h = 0.1$ m, $t = 0.08$ m

boundary conditions: simply supported beam subjected to a constant pressure load p_z at a part of the top of the beam (cf. Fig. 20 (left))

material properties:

(i) unidirectional (denoted UD): same material as in Section 4.1

(ii) foam-made core with $E_{foam} = 50$ MPa, $\nu_{foam} = 0.25$

(iii) $[-45°/45°]$ thin layers that coat the foam: same material as in Section 4.1

2D cross-section mesh: cf. Fig. 20 (right)

results: Displacements and stresses cross-section are given. 3D FEM solution is used as reference one.

25 couples are built to obtain the solution. Figs. 21(a) and 22(a) represent the distribution of the displacements through the cross-section at $x = 0$ and $x = L/2$, respectively. We clearly see the complex variation of these quantities and the excellent agreement with the

Fig. 16. $\sigma_{11}(x = L/2, y, z)$ - Z-shaped beam.

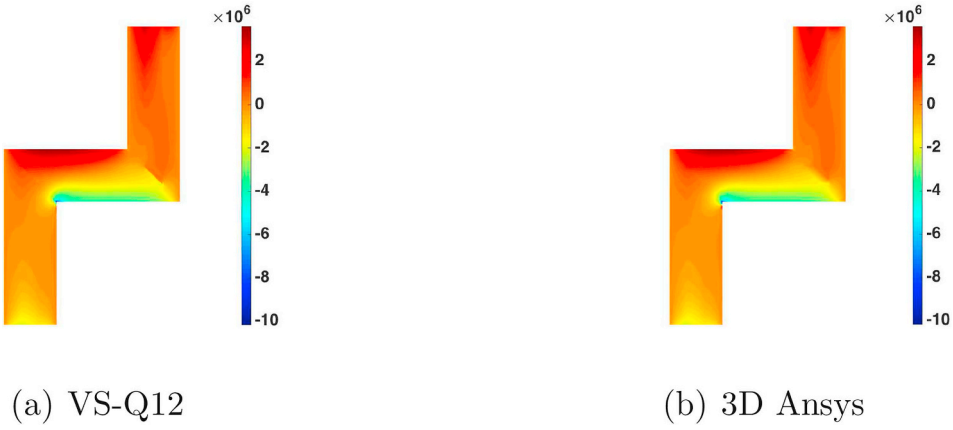

Fig. 17. $\sigma_{12}(x = 0, y, z)$ - Z-shaped beam.

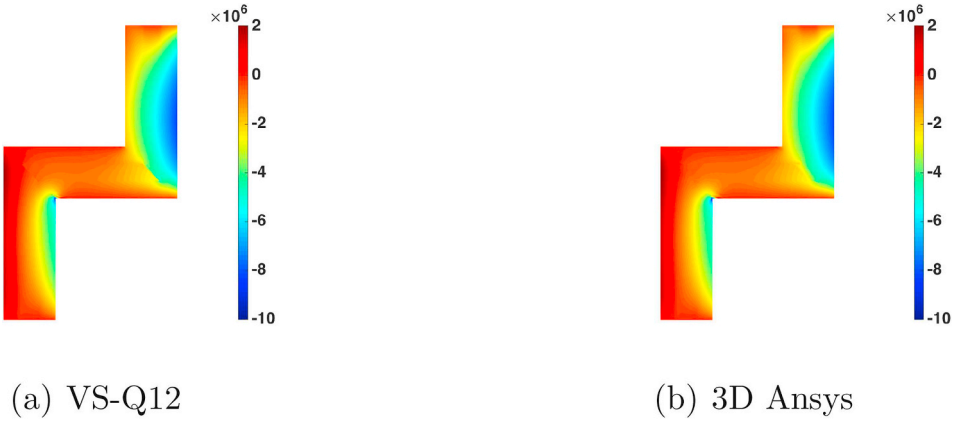

Fig. 18. $\sigma_{13}(x = 0, y, z)$ - Z-shaped beam.

reference 3D results given in Figs. 21(b) and 22(b). Due to the location of the load, the displacement is higher in the left upper part of the cross-section. The in-plane and transverse shear stress are also given in Figs. 23 and 24. It can be inferred from these figures that the method has the capability to capture both the 3D state of stress and the localisation of the steep stress gradient through the cross-section. In the different parts of the structures, the distributions of the mechanical quantities are rather different and classical models have not the capability to represent that.

5. Conclusion

In this work, a higher-order one-dimensional beam finite elements has been developed in the framework of a Proper Generalized Decomposition, a variable separation method that allows us to reduce the computational costs inherent to higher-order models. The displacement field has been approximated over the cross-section based on two different interpolation orders so as to derive kinematic models able to account for non-classical effects such as shear deformation and in- and out-of-plane warping. The approach has been studied and assessed on a wide range of sandwich/laminated composite cross-section geometries for static analysis. These test cases involve bending as well as

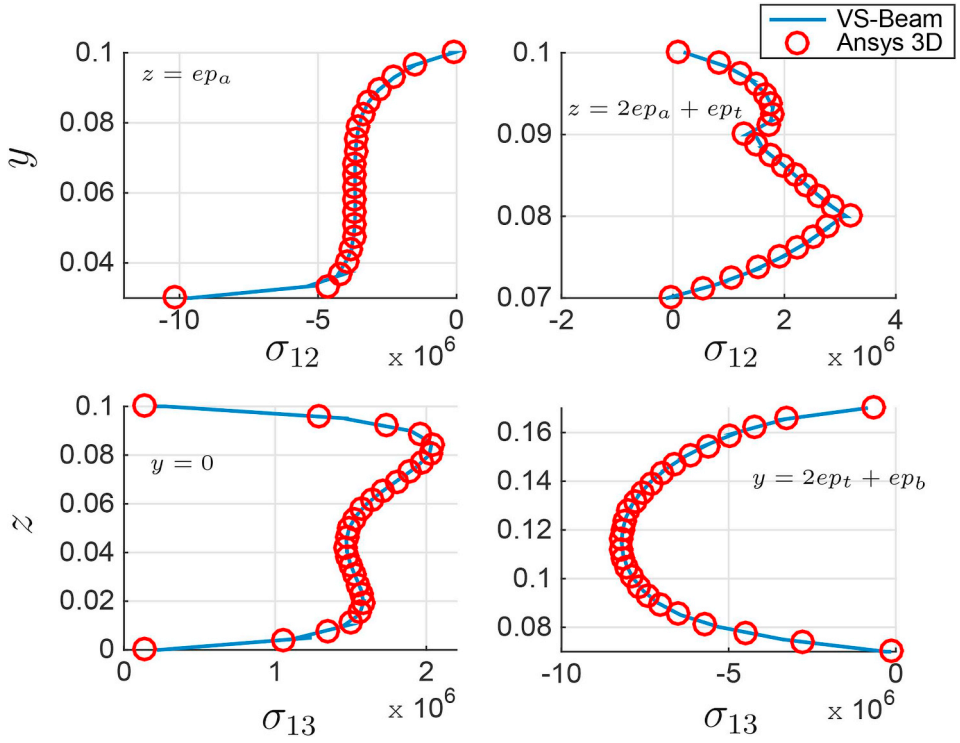

Fig. 19. Distribution of σ_{12} (upper), σ_{13} (lower) - Z-shaped beam.

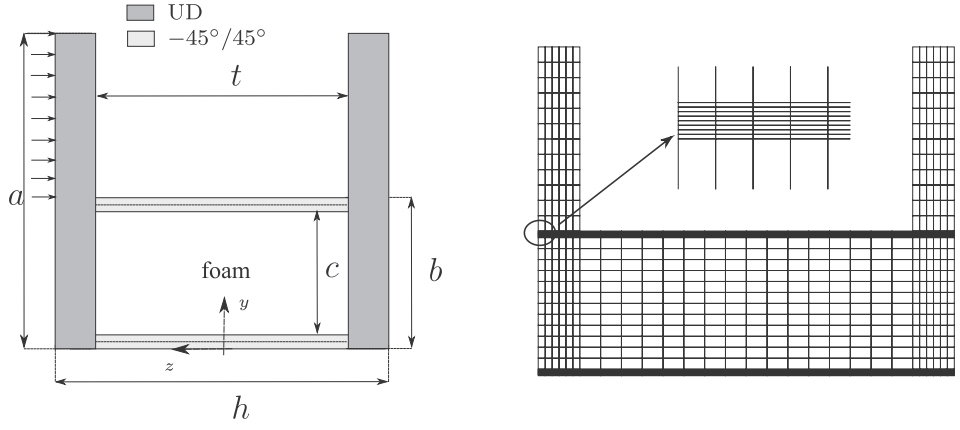

Fig. 20. Longeron beam (left) - 2D mesh (right).

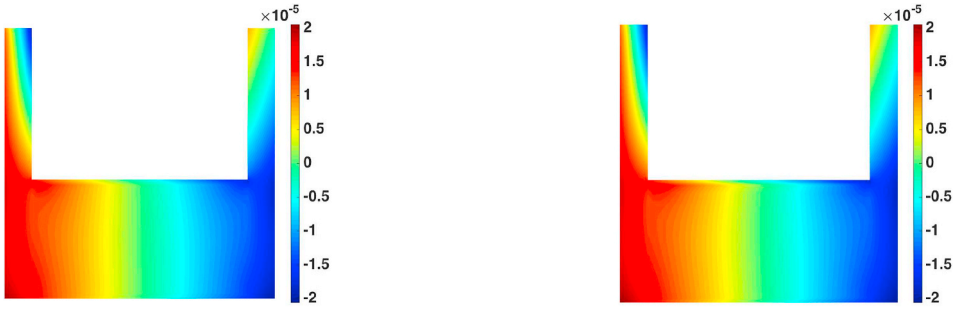

Fig. 21. $u_1(x = 0, y, z)$ - Longeron.

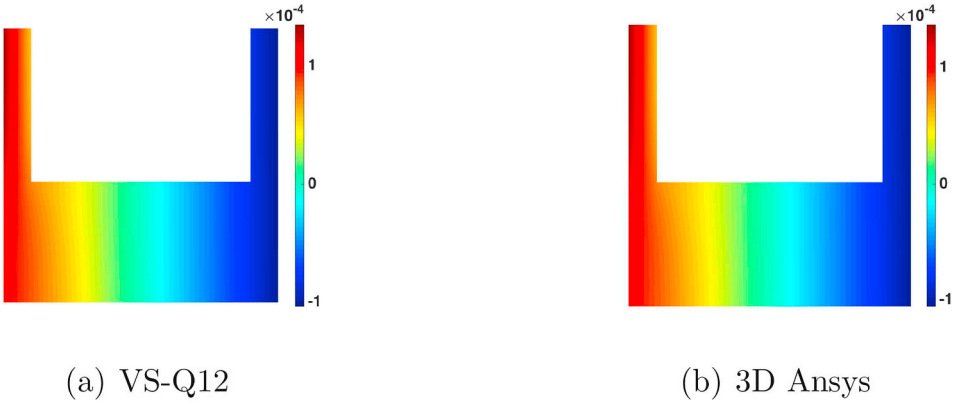

Fig. 22. $u_3(x = L/2, y, z)$ - Longeron.

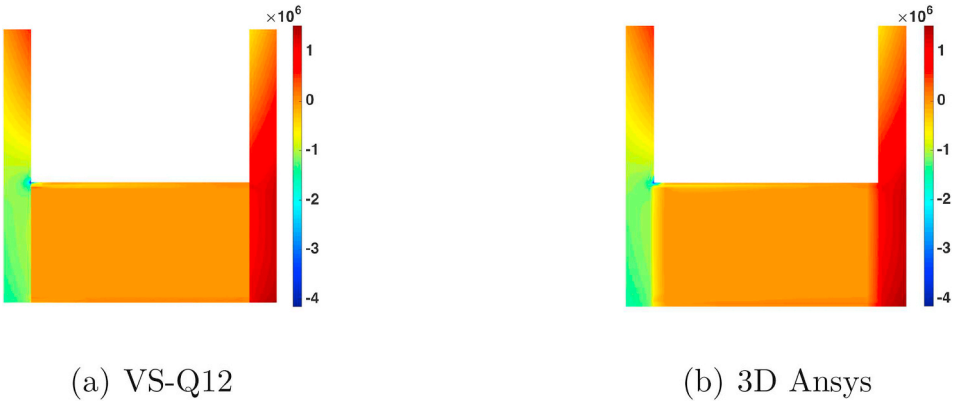

Fig. 23. $\sigma_{11}(x = L/2, y, z)$ - Longeron.

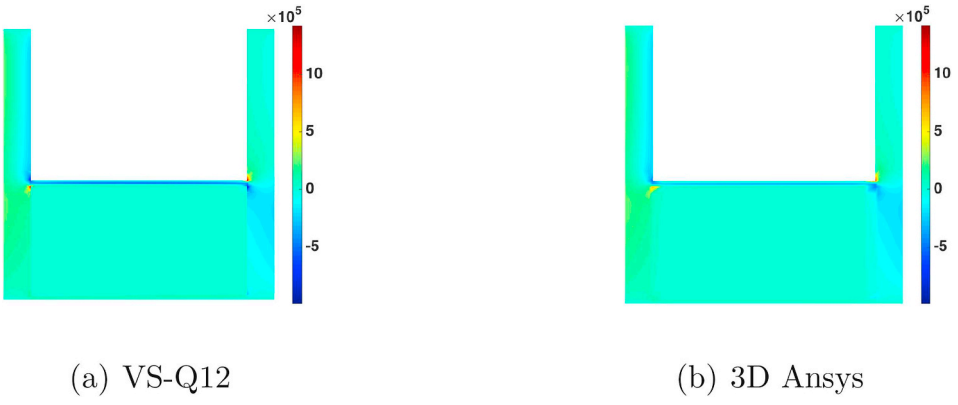

Fig. 24. $\sigma_{13}(x = 0, y, z)$ - Longeron.

bending-torsion loads. It can be highlighted the need to use higher-order interpolation through the cross-section for the displacements. The presented results also showed that quasi three-dimensional solutions for both displacement and stress components can be obtained. Moreover, the localisation of stresses due to the sharp corners is well-captured. Finally, all these features make the present approach very attractive for the modeling of composite beams with any cross-section geometries.

References

[1] Carrera E, Giunta G, Petrolo M. Beam structures: classical and advanced theories. John Wiley & Sons; 2011.

[2] Carrera E, Giunta G, Nali P, Petrolo M. Refined beam elements with arbitrary cross-section geometries. Comput Struct 2010;88:283–93.

[3] Hui Y, Giunta G, Belouettar S, Huang Q, Hu H, Carrera E. A free vibration analysis of three-dimensional sandwich beams using hierarchical one-dimensional finite elements. CPB 2017;110:7–19.

[4] Ammar A, Mokdada B, Chinesta F, Keunings R. A new family of solvers for some classes of multidimensional partial differential equations encountered in kinetic theory modeling of complex fluids. J Non-Newtonian Fluid Mech 2006;139:153–76.

[5] Ammar A, Mokdad B, Chinesta F, Keunings R. A new family of solvers for some classes of multidimensional partial differential equations encountered in kinetic theory modelling of complex fluids: Part II: transient simulation using space-time separated representations. J Non-Newtonian Fluid Mech 2007;144(2–3):98–121.

[6] Ladevèze P. Nonlinear computational structural mechanics: new approaches and non-incremental methods of calculation. Springer Science & Business Media; 2012.

[7] Néron D, Ladevèze P. Proper generalized decomposition for multiscale and multi-physics problems. Arch Comput Methods Eng 2010;17(4):351–72.

[8] F. Chinesta, P. Ladevèze, Separated representations and PGD-based model reduction, Fundamentals and Applications, International Centre for Mechanical Sciences, Courses and Lectures 554.

[9] Nouy A. Proper generalized decompositions and separated representations for the numerical solution of high dimensional stochastic problems. Arch Comput Methods Eng 2010;17(4):403–34.

[10] Chinesta F, Ammar A, Leygue A, Keunings R. An overview of the proper generalized

decomposition with applications in computational rheology. J Non-Newtonian Fluid Mech 2011;166(11):578–92.
[11] Chinesta F, Leygue A, Bognet B, Ghnatios C, Poulhaon F, Bordeu F, Barasinski A, Poitou A, Chatel S, Maison-Le-Poec S. First steps towards an advanced simulation of composites manufacturing by automated tape placement. Int J Material Form 2014;7(1):81–92.
[12] Quesada C, Alfaro I, González D, Cueto E, Chinesta F. PGD-based model reduction for surgery simulation: solid dynamics and contact detection. International symposium on biomedical simulation. Springer; 2014. p. 193–202.
[13] Quesada C, González D, Alfaro I, Cueto E, Chinesta F. Computational vademecums for real-time simulation of surgical cutting in haptic environments. Int J Numer Methods Eng 2016;108(10):1230–47.
[14] Nouy A. A priori model reduction through proper generalized decomposition for solving time-dependent partial differential equations. Comput Methods Appl Mech Eng 2010;199(23–24):1603–26.
[15] Chinesta F, Leygue A, Bordeu F, Aguado JV, Cueto E, González D, Alfaro I, Ammar A, Huerta A. Pgd-based computational vademecum for efficient design, optimization and control. Arch Comput Methods Eng 2013;20(1):31–59.
[16] Chinesta F, Cueto E. PGD-based modeling of materials, structures and processes. Springer; 2014.
[17] Vitse M, Néron D, Boucard P. Virtual charts of solutions for parametrized nonlinear equations. Comput Mech 2014;54(6):1529–39.
[18] Badías A, González D, Alfaro I, Chinesta F, Cueto E. Local proper generalized decomposition. Int J Numer Methods Eng 2017;112(12):1715–32.
[19] Huerta A, Nadal E, Chinesta F. Proper generalized decomposition solutions within a domain decomposition strategy. Int J Numer Methods Eng 2018;113(13):1972–94.
[20] Bognet B, Bordeu F, Chinesta F, Leygue A, Poitou A. Advanced simulation of models defined in plate geometries: 3D solutions with 2D computational complexity. Comput Methods Appl Mech Eng 2012;201–205:1–12.
[21] Bognet B, Leygue A, Chinesta F. Separated representations of 3D elastic solutions in shell geometries. Adv Model Simulat Eng Sci 2014;1(1):4.
[22] Chinesta F, Leygue A, Beringhier M, Tuan Nguyen L, Grandidier J-C, Schrefler B, Pesavento F. Towards a framework for non-linear thermal models in shell domains. Int J Numer Methods Heat Fluid Flow 2013;23(1):55–73.
[23] Reddy JN. Mechanics of laminated composite plates and shells: theory and analysis. CRC press; 2004.
[24] Cueto E, González D, Alfaro I. Proper generalized decompositions: an introduction to computer implementation with Matlab. Springer; 2016.
[25] Vidal P, Gallimard L, Polit O. Assessment of a composite beam finite element based on the proper generalized decomposition. Compos Struct 2012;94(5):1900–10. https://doi.org/10.1016/j.compstruct.2011.12.016.
[26] Vidal P, Gallimard L, Polit O. Proper generalized decomposition and layer-wise approach for the modeling of composite plate structures. Int J Solid Struct 2013;50(14–15):2239–50. https://doi.org/10.1016/j.ijsolstr.2013.03.034.
[27] Vidal P, Gallimard L, Polit O. Robust layerwise C^0 finite element approach based on a variable separation method for the modeling of composite and sandwich plates. Finite Elem Anal Des 2018;139:1–13.
[28] Vidal P, Gallimard L, Polit O. Shell finite element based on the proper generalized decomposition for the modeling of cylindrical composite structures. Comput Struct 2014;132:1–11.
[29] Vidal P, Gallimard L, Polit O. Multi-resolution strategies for the modeling of composite shell structures based on the variable separation method. Int J Numer Methods Eng 2019. https://doi.org/10.1002/nme.5978.
[30] Vidal P, Gallimard L, Polit O. Modeling of composite plates with an arbitrary hole location using the variable separation method. Comput Struct 2017;192:157–70.
[31] Vidal P, Gallimard L, Polit O. Explicit solutions for the modeling of laminated composite plates with arbitrary stacking sequences. Compos B Eng J 2014;60:697–706.
[32] Polit O, Gallimard L, Vidal P, D'Ottavio M, Giunta G, Belouattar S. An analysis of composite beams by means of hierarchical finite elements and a variables separation method. Comput Struct 2015;158:15–29. https://doi.org/10.1016/j.compstruc.2015.05.033.
[33] Giunta G, Belouettar S, Polit O, Gallimard L, Vidal P, D'Ottavio M. Hierarchical beam finite elements based upon a variables separation method. Int. J. Applied Mech 2016;8(02):1650026.
[34] Chinesta F, Ladeveze P, Cueto E. A short review on model order reduction based on proper generalized decomposition. Arch Comput Methods Eng 2011;18(4):395.
[35] Pagano N. Exact solutions for composite laminates in cylindrical bending. J Compos Mater 1969;3:398–411.
[36] Giunta G, Belouettar S, Nasser H, Kiefer-Kamal E, Thielen T. Hierarchical models for the static analysis of three-dimensional sandwich beam structures. Compos Struct 2015;133:1284–301.
[37] Carrera E, Petrolo M. Refined one-dimensional formulations for laminated structure analysis. AIAA J 2012;50(1):176–89.